UC Irvine
UC Irvine Previously Published Works

Title
Analysis of the Puzzling Exchange-Coupling Constants in a Series of Heterobimetallic Complexes

Permalink
https://escholarship.org/uc/item/0vd836mr

Journal
Inorganic Chemistry, 58(14)

ISSN
0020-1669

Authors
Biswas, Saborni
Lau, Nathanael
Borovik, AS
et al.

Publication Date
2019-07-15

DOI
10.1021/acs.inorgchem.9b00757

Peer reviewed

eScholarship.org Powered by the California Digital Library
University of California

Author Manuscript

Author Manuscript

Author Manuscript

Author Manuscript

HHS Public Access

Author manuscript

Inorg Chem. Author manuscript; available in PMC 2019 October 12.

Published in final edited form as:

Inorg Chem. 2019 July 15; 58(14): 9150–9160. doi:10.1021/acs.inorgchem.9b00757.

Analysis of the Puzzling Exchange-Coupling Constants in a Series of Heterobimetallic Complexes

Saborni Biswas[‡], **Nathanael Lau**[¶], **A. S. Borovik**[¶], **Michael P. Hendrich**[*,‡], **Emile L. Bominaar**[*,‡]

[‡] Department of Chemistry, Carnegie Mellon University, 4400 Fifth Avenue, Pittsburgh, Pennsylvania 15213, United States

[¶] Department of Chemistry, University of California–Irvine, 1102 Natural Sciences II, Irvine, California 92697, United States

Abstract

The exchange-coupling constants (J) in a series of bimetallic complexes with an $M^{2+}(\mu\text{-}OH)Fe^{3+}$ core (M = Mn, Fe, Ni, and Cu; series 1), which were reported in a recent study (Sano et al. *Inorg. Chem.* **2017**, 56, 14118–14128), have been analyzed with the help of density functional theory (DFT) calculations. The experimental J values of series 1 showed the remarkable property that they were virtually independent of metal M. This behavior contrasts with that observed for a related series of complexes with $M^{2+}Fe^{3+}$ cores reported by Chaudhuri and co-workers (Biswas et al. *Inorg. Chem.* **2010**, *49,* 626–641) (series 2) in which J increases toward the upper end of the series. Broken symmetry DFT calculations for J, which yielded values in good agreement for the MnFe and NiFe complexes of series 1, gave for the CuFe complex a J value that was persistently much larger than that obtained from the experiment. Attempts to bridge the discrepancy by invoking various basis sets and corrections for hydrogen-bonding effects on J were not successful. The J values for series 1 were subsequently analyzed in the context of an exchange pathway model. From this analysis, it emerged that, in addition to the regular 2e-pathways, which contribute antiferromagnetic terms to J, there are also 3e-pathways that contribute ferromagnetic terms and have the propensity to keep J constant along series 1. It is shown that, while DFT evaluates the 2e-pathway terms reliably, this method seriously underestimates the 3e-pathway contributions, resulting in a too high J value for the CuFe complex of series 1. The pathway analysis of series 2 reveals that the 3e-pathway contributions to J are considerably smaller than those in series 1, resulting in J values that increase toward the upper end of the series, in accordance with the experiment.

[*] **Corresponding Authors** hendrich@andrew.cmu.edu (M.P.H.). eb7g@andrew.cmu.edu (E.L.B.).

ASSOCIATED CONTENT

Supporting Information

The Supporting Information is available free of charge on the ACS Publications website at DOI: 10.1021/acs.inorg-chem.9b00757. Details of the statistical model (Section S1); free-ion electron-transfer energies (Section S2); TD-DFT analysis of 3e-pathways (Section S3); 3e-pathway contributions estimated from free-ion excitation energies (Section S4); pathway analysis of series 2 (Section S5); validity of expression for J_{DFT} (Section S6); analysis of Table 3 of ref 59 (Section S7); assessment of accuracy of B3LYP results for J obtained with basis set 4 (Section S8); comment on inequality $U_{3e} < U_{2e}$ (Section S9) (PDF)

The authors declare no competing financial interest.

Author Manuscript Author Manuscript Author Manuscript Author Manuscript

Graphical Abstract

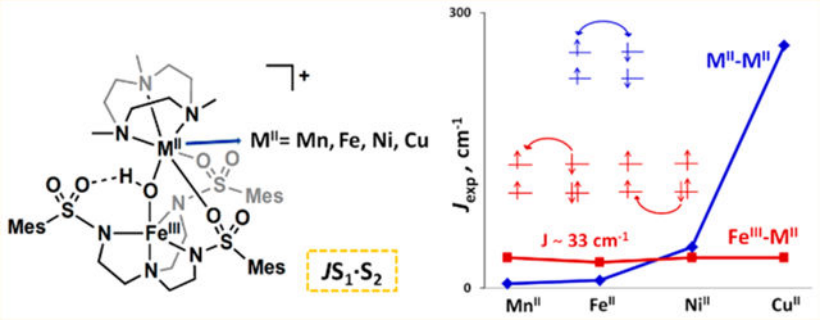

INTRODUCTION

Metalloenzymes containing heterobimetallic active sites assist biological organisms in performing several important reactions. For example, the MnFe site in ribonucleotide reductase catalyzes the synthesis of deoxyribonucleotides;[1] the NiFe site of [NiFe] hydrogenase reversibly forms hydrogen molecules using protons,[2] and the ZnFe site in purple acid phophatase degrades organophosphates.[3] The two metal centers in heterobimetallic active sites often have different coordination spheres and are bridged by one or more oxido or hydroxido ligands. Synthetic heterobimetallic species, with both symmetric[4–14] and asymmetric[15–26] coordination sites, have been prepared as structural or functional models for these active sites. We recently reported the synthesis and the structural and spectroscopic characterization of the bimetallic compounds of the form (MST)Fe^{3+}-(μ-OH)-M^{2+}(TMTACN), using the ligands *N,N′,N″*-[2,2′,2″-nitrilotris(ethane-2,1-diyl)]-tris-(2,4,6-trimethyl-benzene-sulfonamido) (MST^{3-}) and 1,4,7-tetramethyl triaza-cyclonane (TMTACN) and the metals M^{2+} = Mn^{2+}, Fe^{2+}, Ni^{2+}, or Cu^{2+} (series 1), Figure 1.[27] These complexes are rare examples of systems in which the bridging ligand forms an intramolecular hydrogen bond. Hydrogen bonds involving the bridging ligand are also observed in the di-iron centers of the oxygen transporter hemerythrin (Hr) and the O_2/NO reductase flavin di-iron protein (FDP).[28,29]

The complexes in series 1 have similar structures that display only modest variations mainly in the metal–ligand distances. Both the Fe^{3+} and M^{2+} sites in series 1 are high-spin and antiferromagnetically coupled, resulting in net spin states with S = 0, ½, 3/2, and 2 for the $M^{2+}Fe^{3+}$ complexes with M = Mn, Fe, Ni, and Cu, respectively.[27] Variable-temperature EPR spectroscopy of the complexes in series 1 yielded values for the exchange-coupling constants (J) of these species.[27] Surprisingly, the J-values in series 1 were found to be nearly independent of divalent metal ion: J = 35, 26, 35, and 33 cm^{-1} for M = Mn, Fe, Ni, and Cu, respectively (J values are reported here in the convention $J\boldsymbol{S}_M\text{-}\boldsymbol{S}_{Fe}$). The 3d-orbital occupation changes significantly throughout the series, and the expectation is that J should also change significantly as the electrons in the singly occupied orbitals contributing to J are paired off. The near invariance of J in series 1 contrasts with the monotonous increase of this parameter for the heterobimetallic complexes $(MeImA)_3M^{2+}Fe^{3+}$(TMTACN) (M = Mn, Ni, and Cu) reported by Chaudhuri and co-workers,[30] in which the metal sites are triply bridged by the NO-oximato groups of the three 1-methylimidazole-2-aldoximato (MelmA) ligands

Author Manuscript Author Manuscript Author Manuscript Author Manuscript

of M (series 2; the $Fe^{2+}Fe^{3+}$ complex, also reported, is not of interest here because the Fe^{2+} site is low spin). The two-atom bridges in these face-shared complexes prevent metal–metal bonds and mediate superexchange interactions between the metal sites. The *J* values for series 2 are 15, 57, and 76 cm^{-1} for M = Mn, Ni, and Cu, respectively.[30] An increasing value for *J* along the 3d series is a common feature of homometallic compounds.[31–40]

To acquire insight into the *J* values of the two heterobimetallic series, the invariance for series 1 and the effect of the hydrogen bonding on *J*, we have performed density functional theory (DFT) calculations of the broken symmetry type to predict the value of *J*.[41] These attempts were fairly successful, except in the case of the CuFe complex for which J_{DFT} was persistently calculated to be significantly higher than J_{exp}. Thus, somewhat disappointingly, instead of answering the question as to why J_{exp} is invariant in series 1, our DFT calculations raised the additional question as to why J_{DFT} is not. In search of the cause for the invariance of *J* in series 1, we resorted to earlier valence-bond type models for describing *J*.[37,42–50]

In addition to being heterobimetallic, the complexes in series 1 and 2 are mixed valence (+2, +3), a condition which lowers the energy of $M^{2+} \rightarrow Fe^{3+}$ electron-transfer configurations that interact with the electronic ground configuration. As the strength of these interactions depends on the spin state of the complex, they contribute to the energy differences between the spin states and, consequently, to the *J*. Among these electron-transfer configurations are those that result from the transfer of an unpaired electron initially on M and which give rise to the familiar antiferromagnetic 2e-pathway contributions to *J* (Figure 2).[44,46,48] Here, it is argued that in addition to the contribution to *J* from the aniferromagneiic 2e-pathways, there is also a ferromagnetic contribution from 3e-pathways (Figure 2),[51,52] in the case that M is Fe, Ni, or Cu. The spin coupling resulting from 3e-pathways has been referred to as double exchange in the literature and plays an important role in shaping the magnetic properties of homonuclear mixed-valence systems such as iron–sulfur clusters.[41,53–55] Our estimates of the 3e-pathways show that their contributions to the *J* values of series 1 are significant and increase in strength in passing from Mn to Cu, compensating (and in the case of series 1 even canceling) the increase of the net 2e-pathway contribution to *J*. This analysis suggests that the DFT calculations have underestimated the 3e-pathway contributions to the *J*, leading to an overestimation of the *J* value, particularly in the case of the CuFe complexes in which the 3e-pathway contributions reach their maximum value in series 1 and 2. This suggestion has been tested with the help of time-dependent (TD) DFT calculations for the CuFe complex of series 1. Finally, the different trends displayed by *J* along series 1 and 2 have been discussed from a structural perspective in the context of the pathway model.

METHODS

The DFT calculations were performed with Gaussian ‘09,[56] using the functional B3LYP.[57,58] The *J* values were calculated with the expression $J = 2(E_f - EBs)/n_{II}n_{III}$ where n_{II} and n_{III} are the number of unpaired electrons on ions M^{II} and Fe^{III}, respectively, and E_F and E_{bs} are the energies for the optimized geometries of the ferromagnetic (F) and the broken symmetry (BS) configuration, unless explicitly stated otherwise. This expression for *J* follows from the expression $J = 2(E_F - E_{BS})/(\langle \boldsymbol{S}^2 \rangle_F - \langle \boldsymbol{S}^2 \rangle_{BS})_{DFT}$ by replacing the

Author Manuscript Author Manuscript Author Manuscript Author Manuscript

denominator with the product $n_{II}n_{III}$. This approximation is accurate within 0.6% (see Table S11). Hybrid density functionals, among them B3LYP, have been reported to perform better than pure functionals in BS calculations of J.[55,59] In the same report, the root mean square deviation (RSMD) between experimental and B3LYP computed J values for a test set containing 25 oligonuclear transition-metal complexes was found to be rather large, 142 cm $^{-1}$ in our J convention. The mean absolute deviation (MAD, $|J_{exp} - J_{theor}|_{av}$) for the same data set, although somewhat smaller than the RMSD, is still sizable, 93 cm^{-1}. In Section S7, it is shown that this large value mainly results from a few outliers, complexes for which the J values calculated for the X-ray diffraction (XRD) structure and the DFT-optimized structure significantly differ. Excluding those ambiguous cases from the validation of the theory reduces the deviations considerably to RMSD 24 cm^{-1} and MAD 19 cm^{-1}. In our previous work,[29] satisfactory J values were obtained with functional B3LYP, using basis set 6–311G for nonheme di-iron complexes.[60,61] However, this basis set gives for the heterodimers of series 1 values for J that are 2 to 5 times the experimental magnitude. To improve agreement with the experiment, various basis sets have been tested for the MnFe complex of series 1 (Table 1). For the sake of computational expediency, the basis set was only modified at a limited number of atoms (basis sets 3 and 4 of Table 1). The affected atoms include the metal ions and the atoms of the OH bridge, which are critical for the superexchange coupling, and the atoms of the sulfonamido groups to allow for a proper description of the hexavalency of the S atoms. The latter requirement was achieved by using the Triple Zeta Valence Polarization (TZVP) basis[62–64] for the S atoms in basis sets 2, 3, and 4. The extension of the triple-ζ-basis set (6–311G, basis set 1) with polarization functions (TZVP, basis set 2) at all atoms lowered J by 17%. The same lowering was obtained when the extension was made at the selected atoms (basis set 3), justifying the use of a smaller, hybrid basis set for the purpose of calculating J. This result is consistent with an earlier report.[59] The J value for basis set 3 was lowered an an additional 8% by introducing the effect of the solvent, using the Polarizable Continuum Model (PCM) module of G'09 (basis set 3, ε = 8.93). To include the effect of the relativistic contraction of the core electron orbitals and avoid the disbalance its neglect may cause on the effective potentials acting on the 3d-electrons in the heterobimetallic complexes, the Stuttgart Dresden (SDD) pseudopotential basis[65–71] has been used for the metal ions in basis set 4. The change to the SDD basis at the metal ions resulted in a 12% decrease in J compared to values obtained for basis 3. The J value obtained with basis set 4 and ε = 8.93 gives the closest match with experiment. In the next section, the utility of basis set 4 (ε = 1) has first been tested in the prediction of J values for several synthetic homo- and heterobimetallic complexes before being applied to the complexes of series 1 (ε = 8.93). The optimized structures and the Mulliken spin populations of the metal ions for the F and BS states were found to be nearly identical, apart from a sign flip in the population of the minority-spin site. These properties are typical for the DFT solutions of exchange-coupled systems. Except for one case, the DFT optimized structures are in good agreement with those obtained from XRD (see below).

The best basis set (basis set 4) emerging from the above analysis has been used for calculating the J values for structurally and magnetically characterized homobimetallic[72–79] as well as heterobimetallic[6,80–83] complexes with hydroxo/alcoxo/carboxylate bridges to test its utility for a wider range of systems. The results of these calculations are presented in

Author Manuscript Author Manuscript Author Manuscript Author Manuscript

Section S8. The calculations were performed in gas phase ($\varepsilon = 1$) because the experimental J values for all these complexes were obtained from polycrystalline/amorphous solid samples. The homobimetallic test set contained 8 complexes with experimental J values ranging from 15 to 43 cm^{-1} (see Table S12 and Figure S11) and gave a MAD of 5 cm^{-1}. The heterobimetallic test set contained 7 complexes with experimental J values ranging from –105 to 78 cm^{-1} (see Table S13 and Figure S12) and gave a MAD of 11 cm^{-1}, compatible with the MAD for the reduced data set of ref 59 (see above).

RESULTS

Having established the accuracy of basis set 4 in the calculation of J values for a wide range of complexes, we now proceed with calculating the J values for the remaining complexes of series 1. The results of these calculations are given in Table 2 in the first column under the header J_{DFT}. The values are 27%, 81%, 51%, and 327% greater than J_{exp} for the MnFe, FeFe, NiFe, and CuFe complexes, respectively, and show a moderate increase in J_{DFT} from MnFe to NiFe followed by a dramatic jump for CuFe. In contrast, J_{exp} remains virtually constant throughout the heterometallic series. Thus, although the use of basis set 4 predicts many experimental J values with reasonable accuracy, our DFT calculations have not succeeded in describing the invariance of J along series 1, particularly not in the case of the CuFe complex. More specifically, the value $J_{exp} = 33$ cm^{-1} for the CuFe complex lies well outside the range 141 ± 11 cm^{-1} around the J_{DFT} suggested by the MAD of the heterobimetallic test set (Figure S7). To improve upon this unsatisfactory situation, we have first revisited the experimental results and then explored several alternative causes for the discrepancy between J_{exp} and J_{DFT}. The results of the efforts have been discussed in the following subsections.

Verification and Additional Evidence for the Low Value of J_{exp} for CuFe Complex.

The J_{exp} value for the CuFe complex of series 1, given in Table 2, was obtained from a solution sample in 50:50 DMF/THF. To both verify and obtain additional evidence for the low J_{exp} value previously reported for the CuFe species, measurements were repeated for the powder form of this complex. The EPR signals from this sample are shown in Figure 3 for temperatures of 10 and 157 K. The signal at 10 K has a feature at $g = 10.6$ similar to the signal from the solution sample.[27] The spectrum has an additional feature at low magnetic field with the same temperature dependence, which we attribute to intermolecular magnetic dipolar interactions in powder. At higher temperatures, a new feature was observed at $g = 14.6$ as shown in Figure 3. This feature, which was too broad for detection in solution, allowed a direct probe of the excited $S = 3$ state of the exchange-coupled CuFe complex. A series of spectra was recorded over a temperature range of 10 to 157 K. The intensity of the $g = 14.6$ feature was measured and is plotted in the inset of Figure 3 as the product of signal intensity times temperature versus temperature. The plotting of this product (rather than signal intensity) removes the overwhelming $1/T$ Curie law dependence, thereby accentuating the effect of the exchange interaction on the data. The fit overlaid on the data of the inset is for the population of the $S = 3$ multiplet using a value for J of 35(5) cm^{-1}, in agreement with the previous value for the complex in DMF/THF (Table 2).

Author Manuscript Author Manuscript Author Manuscript Author Manuscript

Effect of Structural Discrepancies on *J*.

Table 3 shows a comparison of selected geometric parameters obtained from XRD and DFT optimization of the complexes of series 1. The comparison shows that the bond distances and angles obtained from DFT are only marginally higher than their counterparts from XRD. Consequently, the *J* values calculated for the DFT-optimized structure and the XRD structure of the CuFe complex are almost equal: J_{DFT} = 141 cm^{-1} and J_{DFT}^{XRD} = 138 cm^{-1}. Thus, differences between J_{exp} and J_{DFT} cannot be ascribed to discrepancies between the XRD and DFT structures. The structural parameters in the XRD and DFT structures show similar trends across series 1. In both data sets, the Fe1–M1 and O1–O6 distances are nearly constant; the M1–O1 distance decreases from Mn to Cu, and the Fe1–O1– M1 bond angle increases by 4° from Mn to Cu in both the XRD and DFT structures.

Effect of H-Bonding on *J*.

The recognition that hydrogen bonds (H-bond) affect *J*[28,29,84,85] raises the possibility that the discrepancy between J_{exp} and J_{DFT} in series 1 may arise from inaccuracies in the DFT assessment of the H-bond donated by the hydroxido bridge to one of the sulfonamido oxygens (see Figure 1). This H-bond weakens the covalent O–H-bond in the hydroxo group and increases *J* by conferring some oxido-character to the bridge. Thus, an overestimation of the H-bonding would lead to a spurious increase in the *J* value and could be a potential cause for the discrepancy between the calculated and observed values for this parameter. Attempts to improve the description of the H-bond by introducing a dispersion correction to the DFT calculations,[86] using option GD3BJ of Gaussian ‘09, resulted in a decrease of the HO…O=S distance from 2.67 to 2.57 Å and gave an even larger value for J_{DFT} (159 cm^{-1}). To estimate the net H-bond effect on J_{DFT}, calculations were performed on abridged structures obtained by removal of the H-bond from the optimized geometries of the complete molecules.

In a first set of calculations, the N4–S (sulfonamido) bond was cleaved by replacing the sulfonamido group by an H atom placed at the common H–N distance from atom N4, yielding the truncated structure of Figure 4a. The *J* values were then calculated from the E_F and E_{BS} values obtained from single point calculations as described in the Methods (Table 2). Attempts to reoptimize the truncated structure resulted in a loss of the geometric integrity of the $[MST]^{3-}$ ligand and were abandoned. Table 2 shows that the loss of the H-bond has lowered the *J* values and brought them into the experimental ranges for the MnFe, FeFe, and NiFe complexes (Table 2), suggesting that the DFT calculations presented here have overestimated the strength of the H-bond in these species. However, the discrepancy for the CuFe complex persists (Table 2). In search of what caused the overestimation, we have recalculated the *J* value for the truncated structure of the CuFe complex, using a basis set in which the orbitals of the atoms removed in the truncation were retained as “ghost” orbitals. However, the addition of the ghost orbitals changed J_{DFT} (truncated) by as little as 0.4 cm^{-1}, showing that the truncation induced lowering of *J* is not due to a basis set superposition error[87,88] in the value for J_{DFT} arising from the orbitals at the vicinal sulfonamide group. A satisfactory explanation for why DFT has overestimated the H-bonding effect on J in series 1 is still pending.

Author Manuscript Author Manuscript Author Manuscript Author Manuscript

In a second set of calculations, the sulfonamido group was rotated 75° over dihedral angle Fe–N4–S–O6 to increase the O1···O6 distance and remove the H-bond (Figure 4b). The resulting structure was reoptimized while keeping the dihedral angle fixed. The *J* values, given in the last column of Table 2, show that H-bond removal by rotation has a smaller effect on *J* than truncation. As a possible explanation for the difference, we suggest that the structural changes caused by the constrained reoptimization have partially compensated for the loss of the H-bond. Obviously, the effect of losing the H-bond on *J* in the second set of calculations is more intricate than in the first set because the absence of the H-bond not only removes the intrinsic effect of the covalent H–O bond weakening, like in the first set of calculations, but also affects the structure of the bridge, which may change *J* as well.

As expected, both procedures for removing the H-bond decrease *J*. The largest H-bond effect is obtained for the FeFe complex (104%, 27%) and the smallest, for the CuFe complex (12%, 15%) for Figure 4a,b. In any event, the removal of the H-bond improves the agreement between J_{DFT} and J_{exp} in series 1, which suggests that DFT has overestimated the H-bonding effect on *J*. The good agreement between J_{exp} and the value for J_{DFT} obtained after removing the H-bond in the MnFe, FeFe, and NiFe complexes of series 1 suggests that the H-bonding effect on *J* in these systems is much smaller than calculated by our DFT calculations, in contrast to the case of the hydroxido-bridged di-iron(III) systems described in the literature[29,85] in which inclusion of H-bonding improved the agreement between J_{DFT} and J_{exp}. The conclusion that the effect of H-bonding on *J* is weak in series 1 is not unexpected given that the covalent S=O bond in the sulfonamido group makes this group a weaker H-bond acceptor than those of nitrate[85] and glutamate.[29]

In summary, the effect of the H-bond on *J* is small and does not explain the large discrepancy between the experimental and DFT-calculated *J* values for the CuFe complex of series 1. This discrepancy is the focus of the following discussion.

DISCUSSION

In the Results section, it was shown that J_{DFT} for the CuFe complex in series 1 is about four times larger than J_{DFT} for the MnFe complex. In contrast, the J_{exp} values for the CuFe and MnFe complexes are equal. In the following discussion, we explore the origins of the invariance of J_{exp}. We use valence-bond type models for *J* to give physical meaning to the underlying calculations.[42–48,89] Wave function based theories for calculating *J* have been reviewed recently.[55] In these models, the exchange interaction between two paramagnetic metal ions with N_A unpaired electrons at site A and N_B unpaired electrons at site B is often written as the sum of 2-electron Hamiltonians for the intermetal exchange couplings between the unpaired electrons at the two metal sites (eq 1).

$$\sum_{i=1}^{N_A}\sum_{k=1}^{N_B} j_{ik}\hat{\mathbf{s}}_i \cdot \hat{\mathbf{s}}_k \equiv \frac{1}{N_A N_B}\sum_{i=1}^{N_A}\sum_{k=1}^{N_B} j_{ik}\hat{\mathbf{S}}_A \cdot \hat{\mathbf{S}}_B = J\hat{\mathbf{S}}_A \cdot \hat{\mathbf{S}}_B \quad (1)$$

Author Manuscript Author Manuscript Author Manuscript Author Manuscript

The one-electron spin operators, $\hat{\mathbf{s}}_i$ can be expressed in terms of the total spin operators for metal sites A and B, $\hat{\mathbf{S}}_X$ (X = A or B), using the Wigner-Eckart theorem,[90] in the calculation of the matrix elements in the direct-product basis $|S_A, M_A\rangle|S_B, M_B\rangle$ ($M_A = -S_A, -S_A + 1, \ldots, S_A$ and $M_B = -S_B, -S_B + 1, \ldots, S_B$) for a bimetallic center with local spins S_A and S_B; this equivalence is indicated by the = symbol in eq 1. The second equality in eq 1 identifies parameter J for the coupling of the net metal spins with the average of the individual exchange-coupling constants, j_{ik}, taken over the 2e-pathways (i,k), connecting unpaired electrons at the two metal centers. A statistical analysis, given in Section S1, demonstrates that invariance would require the J values for the 2e-pathways in series 1 to be distributed in narrow ranges around the experimental value for J. However, in the following discussion, it will be argued that such distributions are unrealistic in the light of both empirical and theoretical evidence, initiating the search for an alternative explanation.

The values of J in homobimetallic systems trend higher toward the end of the 3d series (see below).[31–39,49] The explanation for this trend is that in the Aufbau from coordinated Mn^{2+} to Cu^{2+} the unpaired electrons in the low-lying, weakly antibonding 3d-orbitals are paired off first, confining the remaining unpaired electrons to the more delocalized, higher-lying 3d-orbitals. As the superexchange coupling originates from the overlap between the unpaired electron orbitals of the two metal sites due to the covalent delocalization of these orbitals toward the ligand bridge, the largest j_{ik} values are expected to occur for the orbitals that remain singly occupied all along. In particular, the strongest coupling arises for the unpaired electron orbital of Cu^{2+} ion. Indeed, as it is illustrated in Figure 5, this orbital has a lobe directed toward the hydroxido bridge and has the largest amplitude at the bridge among the 3d-orbitals. The orbital state of the Cu^{2+} ion is firmly locked-in by the structure, and attempts to substantially influence J by making changes to the unpaired electron orbital required unrealistically large distortions of the primary coordination sphere of the Cu^{2+} center. Thus, if one or only a few dominant exchange pathways exist, the sum of eq 1 is determined by these pathways, but the denominator of eq 1 is 5 for $Cu^{2+}Fe^{3+}$ versus 25 for $Mn^{2+}Fe^{3+}$, causing a significant increase in the value of J for $Cu^{2+}Fe^{3+}$ relative to $Mn^{2+}Fe^{3+}$.

With this said, the above expectation is not supported by the experiment. We think this discrepancy is because the model underlying eq 1 is incomplete. The incomplete model is illustrated in the case of a NiFe complex in the top halve of Figure 6 and considers contributions to J from 2e-pathways that result from the interactions of the antiferromagnetic ground state with the configurations resulting from the electron transfers indicated by the blue arrows in diagram D1 of Figure 6. In the spirit of the broken symmetry approach, diagrams D1 and D5 represent the antiferromagnetic $S = 3/2$ ground state by a simple spin configuration in which the spins of the unpaired electrons at Fe^{3+} are up and those at Ni^{2+} are down. As an example, the result of the transfer indicated by the upper blue arrow in diagram D1 is shown in diagram D2. The excitation energy for the transfer, denoted U^{2e}, is much larger than the matrix element connecting the ground state with the electron-transfer state, which is denoted b_{ik} for the orbital pair (i,k), permitting the application of second-order perturbation theory for calculating the contribution of the transfer to J. The matrix element depends sensitively on the bridging-ligand-mediated overlap properties between the

Author Manuscript Author Manuscript Author Manuscript Author Manuscript

unpaired-electron-containing “magnetic” orbitals, labeled *i* and *k*. As the relevant terms in the fundamental Hamiltonian for the transfer process are independent of spin, the orientation of the spin of the transferring electron remains unchanged in the process. For the ferromagnetic state (diagram D4), the same transfer is Pauli forbidden and, consequently, the transfer interactions in the 2e-pathways give exclusively antiferromagnetic contributions to the exchange-coupling constant *J*. More precisely, using the notation $J\hat{\mathbf{S}}_{\mathrm{A}} \cdot \hat{\mathbf{S}}_{\mathrm{B}}$ with A = Fe^{3+} and B = M^{2+}, in second-order perturbation theory, the contribution to J from a 2e-pathway (*i,k*) is given as $J_{ik}^{\mathrm{AF}} = \frac{2}{N_{\mathrm{A}}N_{\mathrm{B}}}\frac{b_{ik}^{2}}{U^{2e}}$, where capital *J* is used to denote the inclusion of factor $1/N_{\mathrm{A}}N_{\mathrm{B}}$. The reverse transfers, Fe → M, of which the result for the top arrow in diagram D1 is shown in diagram D3, have ideally the same b_{ik} values as the M → Fe transfers but have a much larger *U* value due to the greater charge disproportionation (Table S3) and will therefore be further ignored here. In addition to the second-order contributions, there are also zeroth-order contributions that are strictly ferromagnetic and much smaller in magnitude. In his seminal paper, Anderson[46] referred to the ferro- and antiferromagnetic contributions as “potential” and (somewhat confusingly) “kinetic” exchange, respectively, and estimated that the kinetic exchange contribution to a pathway (*i,k*) prevails, unless matrix element b_{ik} vanishes for reasons of symmetry or accidentally. The complexes studied here all lack symmetry between sites; thus, all 2e-pathways (ten pathways in the case of NiFe complex shown in diagram D1) are likely to be antiferromagnetic. For later reference, diagram D5 shows the ideal case of a dimer complex with a linear bridge in which for every orbital *i* on site A there is only one corresponding orbital on site B, say orbital *i′*, for which $b_{ii'} \neq 0$. These pathways give antiferromagnetic (“kinetic”) contributions to *J*, while the remaining pathways ($b_{ij} = 0$, $j \neq i'$) give weak ferromagnetic (“potential”) exchange contributions.

As discussed above, the 2e-pathways are expected to give *J* values for our heterobimetallic $M^{2+}Fe^{3+}$ complexes that increase when M passes from Mn to Cu. The nearly constant experimental *J* values for these species suggest that there are additional ferromagnetic contributions that counter this increase. The 3e-pathways, indicated by the blue arrows in diagram D6, give such contributions.[51,52] The configuration resulting from the transfer indicated by the upper blue arrow in the ferromagnetic configuration of diagram D6 is shown in diagram D7 and features high-spin, Hund’s rule obeying Fe^{2+} and Ni^{3+} sites. A more detailed analysis shows that the 3e-pathway for orbital pair (*i,k*) contributes the ferromagnetic term $\frac{j_{ik}^{\mathrm{F}}}{N_{\mathrm{A}}N_{\mathrm{B}}} = J_{ik}^{\mathrm{F}} = -\frac{N_{\mathrm{B}}}{N_{\mathrm{B}}+1}\frac{2}{N_{\mathrm{A}}N_{\mathrm{B}}}\frac{b_{ik}^{2}}{U^{3e}}$ to *J* in $J\hat{\mathbf{S}}_{\mathbf{A}} \cdot \hat{\mathbf{S}}_{\mathbf{B}}$ which is equal to J_{ik}^{AF} apart from the sign, the factor $N_{\mathrm{b}}/(N_{\mathrm{b}} + 1)$, and the value for the excitation energy. The values for the matrix element b_{ik} in the expressions for $J_{\mathrm{ik}}^{\mathrm{F}}$ and $J_{\mathrm{ik}}^{\mathrm{AF}}$ are assumed to be approximately equal because both F and AF terms involve the same *i*–*k* orbital interactions. A transfer in the 3e-pathway is also allowed in the antiferromagnetic configuration (diagram D8) provided the transferring electron has down spin. However, the configuration resulting from the latter transfer process, shown in diagram D9, features a Ni^{3+} site in a non-Hund state. The excitation energy of a paired electron in the BS state, U_{BS}, resulting in the configuration shown in diagram D9, is higher than the excitation energy of the same electron

Author Manuscript Author Manuscript Author Manuscript Author Manuscript

in the F state, U_F, resulting in the configuration shown in diagram D7. The inequality $U_F < U_{BS}$ implies that a 3e-pathway in the BS state gives a smaller contribution to J than the corresponding 3e-pathway in the F state, together leading to a net ferromagnetic contribution to J (Section S3). Thus, every time that an electron is added to the 3d shell in passing from Mn^{2+} to Cu^{2+}, an antiferromagnetic 2e-pathway contribution to J is eliminated and replaced by a ferromagnetic contribution from a 3e-pathway, and consequently, the value of J does notsignificantly increase. The F and AF exchange contributions relate to the experimental value of J as

$$N_A N_B J_{exp} = N_A N_B j_{av}^{AF} + (25 - N_A N_B) j_{av}^{F} \quad (2)$$

where j_{av}^{AF} is twice the average of the $\frac{b_{ik}^2}{U}$ values and $j_{av}^{F} = -\frac{N_B}{N_B+1}\frac{U^{2e}}{U^{3e}} j_{av}^{AF}$ provided the contributions for the non-Hund states can be ignored (see below). Since U^{2e} and U^{3e} are the transfer energies of the 3d-electrons of metal M belonging to the majority spin and minority spin populations, respectively, we expect them to obey the inequality $U^{2e} > U^{3e}$ (Section S9). This inequality is supported by molecular orbital energies, which are usually higher for the minority spin electrons than for the majority spin electrons, and by TD-DFT calculations (Section S3).

The application of eq 2, using the ratio $U^{2e}/U^{3e} = 2$, is shown in Table 4. The Δ_M values of Table 4 approximate the sum of the 2e-pathways that are eliminated by pairing off an unpaired electron on M relative to the $Mn^{2+}Fe^{3+}$ configuration. The values for j_{av}^{AF} (M) exhibit the increase anticipated for the 2e-pathway contributions for Mn to Cu. The foregoing analysis suggests there are two sets of pathway parameters for a $M^{2+}Fe^{3+}$ complex, one for j_{ik}^{AF} (M) with the average $j_{av}^{AF} > 0$ and the other for j_{ik}^{F}, with the average j_{av}^{F} (M) < 0. The J for the CuFe complex is then the sum over five j_{ik}^{AF} values and 20 j_{ik}^{F}. values, divided by $N_A N_B = 5$. By increasing the number of j_{ik}^{F}. terms along the 3d series, the value for j_{av}^{AF}(M) can increase, in accordance with the expected behavior of this quantity, without changing J.

Hetero- versus Homobinuclear Complexes.

The trend of increasing J along the 3d series in homonuclear compounds is nicely illustrated by the superexchange interactions through linear halide bridges between the metal ions in KMF_3 solids with perovskite structure, M = Mn,…, Cu, which show a pronounced increase in J: 4.3–5.1 cm^{-1} (M = Mn), 8.3 cm^{-1} (Fe), 44–51 cm^{-1} (Ni), and 264 cm^{-1} (Cu),[31–40] in sharp contrast to the near invariance of J in the series of heterometallic $M^{2+}Fe^{3+}$ complexes in series 1. For a comparison of the homo- and heterobimetallic series, we replaced the latter by a hypothetical, linear version and counted the number of comparable ferro- and antiferromagnetic pathways under the constraints on the matrix elements imposed by diagrams D5 and D10 of Figure 6. The result of the count is shown in Table 5 and reveals that for each $Fe^{3+}M^{2+}$ combination the total number of antiferromagnetic contributions in

Author Manuscript Author Manuscript Author Manuscript Author Manuscript

the two series is equal but that the ferromagnetic 3e-pathway contributions, which play a prominent role in the heterobimetallic series 1, are absent in the homobimetallic series. The increasing number of ferromagnetic 3e-pathway contributions to the J values for the heterobimetallic complexes along the 3d series compensates the increasing antiferromagnetic contributions from the 2e-pathways, providing a mechanism by which J remains constant. In contrast, due to the absence of these ferromagnetic "resonance" contributions, the homobimetallic series exhibits the increase in J anticipated for the 2e-pathways. In addition to the ferromagnetic 3e-pathway terms, the heterometallic series has a larger number of "potential exchange" (PE) contributions, providing additional compensation of the antiferromagnetic exchange in the heterometallic series.[46] As it was mentioned above, PE only prevails for pairs of orbitals for which $b_{ik} = 0$ and $= 0$ for reasons of symmetry or accidentally and is a first-order, ferromagnetic contribution to J, distinct from the ferromagnetic second-order contributions to J from 3e-pathways. The sign change of J due to the vanishing of J_{ik}^{AF} is illustrated in the last two rows of Table S13 by two $Cu^{2+}M^{3+}$ complexes with the same ligand system. The CuFe complex has a strong antiferromagnetic coupling owing to antiferromagnetic 2e-pathways linking the unpaired-electron carrying e_g orbitals of the Cu($t_2^6e^3$) and Fe($t_2^3e^2$) centers. The coupling turns ferromagnetic in the CuCr complex because of the absence of 2e-pathways involving e_g orbitals between the Cu($t_{2g}^6e_g^3$) and Cr(t_{2g}^3) centers (see Table S13). The second-order contributions to J for the CuCr species are then dominated by 1e- and 3e-pathway contributions, which are both ferromagnetic. (N.b., the transfer of the unpaired e_g electron on Cu^{2+} to one of the empty e_g orbitals of Cr^{3+} represents a le-pathway.) Together with PE, these contributions yield a ferromagnetic J.

Non-Hund Contributions to 3e-Pathways.

The 3e-pathways in the BS configuration, illustrated in diagrams D8 and D9 of Figure 6, lower the energy of the BS configuration and give thus an antiferromagnetic contribution to J that partially compensates the ferromagnetic 3e-pathway contribution shown in diagrams D6 and D7 of the same figure. In the first approximation, the compensation can be represented by multiplying the 3e-pathway contributions to J in the fifth column of Table 4 with the reduction factor $f = \left[\left(U_F^{3e}\right)^{-1} - \left(U_{BS}^{3e}\right)^{-1}\right] / \left(U_F^{3e}\right)^{-1}$, in which U_F^{3e} and U_{BS}^{3e} are the excitation energies for the Hund and non-Hund configurations ($U_F^{3e} < U_{BS}^{3e}$) like those in diagrams D7 and D9 of Figure 6 (see Section S4). By using free-ion based excitation energies for a $Cu^{2+}Fe^{3+}$ species (Table S8), reduction factor f is calculated to be 0.26 (Table S7) resulting in the antiferromagnetic contribution $J^{AF} = 60\ cm^{-1}$ to J (Table S9). Although this value is lower than the one given in Table 4 for this complex, it is twice the J value for the $Mn^{2+}Fe^{3+}$ complex (Table S9). The increase of J^{AF} along the 3d series is thus retained.

Why is J_{DFT} for the $Cu^{2+}Fe^{3+}$ Complex Higher than J_{exp}?

The DFT calculations for the J values in the heterometallic $M^{2+}Fe^{3+}$ complexes in series 1 were found, albeit after making some adjustments, to be in good agreement with the experimentally determined values for the MnFe, FeFe, and NiFe complexes. However, the J_{DFT} value for the CuFe complex was persistently about four times larger than that observed. This result suggests that the 3e-pathways have been underestimated by DFT. Obviously,

Author Manuscript Author Manuscript Author Manuscript Author Manuscript

nonvanishing 3e-pathway contributions to J require the values for U_F^{3e} and U_{BS}^{3e} to be different ($f = 0$ for $U_F^{3e} = U_{BS}^{3e}$). To test this requirement, a subset of these excitation energies have been estimated with the help of TD-DFT calculations for the F and BS states of the CuFe complex (Section S3). Figures S4 and S5 enabled us to identify similarly shaped 3d-type molecular orbitals in the F and BS states, resulting in the correspondence presented in Table S5. Using this mapping, we were able to establish corresponding Cu → Fe β-electron-transfer processes in the TD-DFT output for the BS and F states (Table S6). The excitation energies for these transitions, also listed in Table S6, are remarkably close, resulting in very small reduction factors ($f \sim 0.06$) for the 3e-pathways (Table S7). The smallness is possibly caused by covalency because the difference between the energies for excitation to non-Hund and Hund states, U_{BS}^{3e} and U_F^{3e}, respectively, depends on intra-atomic exchange integrals of the form $(d_1d_2||d_1d_2)$, which are reduced by the admixture of the 3d-orbitals with ligand-centered orbitals. More specifically, with the replacement of 3d atomic orbitals by 3d-type molecular orbitals of the form $\varphi_i = c_i d_i + s_i L_i$ (L_i is the ligand component of the orbital, and c_i and s_i are mixing coefficients <1), the exchange integral is reduced by a factor smaller than 1, roughly as in $(\varphi_1\varphi_2||\varphi_1\varphi_2) \approx c_1^2 c_2^2\ (d_1d_2||d_1d_2)$. For example, for $c_1 = c_2 = 1/\sqrt{2}$, the reduction factor is 0.25. In contrast to the 3e-pathways, the 2e-pathway contributions to J are unaffected by the covalent reduction of the intra-atomic exchange integrals as the transfer in the F state is strictly forbidden by the Pauli principle ("$U_F^{2e} = \infty$"). Due to the drastic reduction of the ferromagnetic 3e-pathways, J_{DFT} for the CuFe complex is essentially made up of antiferromagnetic 2e-pathway contributions. This result together with the observation that J_{DFT} is higher than J_{exp} lead to the conclusion that the smallness of the 3e-pathway contributions to J_{DFT} is a deficiency of DFT rather than a property of the true CuFe complex.

In our comments about the bottom two complexes of Table S13 (Section S8), we suggested that the ferromagnetic coupling in the CuCr complex is due to a combination of ferromagnetic 1e-pathway, 3e-pathway, and potential exchange contributions. However, if DFT underestimates the ferromagnetic 3e-pathway contributions in the CuCr complex as it does in the CuFe complex of series 1, then the ferromagnetic coupling in this complex, which is accurately reproduced by DFT, must be the result of potential exchange.

Analysis of J_{exp} of Series 2.

In contrast to the nearly constant value for J_{exp} in series 1, the values for J_{exp} in series 2 show a steady increase along the 3d row: J_{Mn} =15 cm^{-1}, J_{Ni} = 57 cm^{-1}, and J_{Cu} = 76 cm^{-1} (Table 6). The pathway analysis of the J_{exp} values for series 2 using eq 2 is given in Table S10 and yields values for Δ_M close to zero, indicating that the 3e-pathway contributions are negligible in these systems (Section S5). Thus, the main difference between the exchange interactions in series 1 and 2 is that the 2e-pathways associated with the t_2 orbitals of Mn in the MnFe species and their associated 3e-pathway contributions in the NiFe and CuFe species are large in series 1 but small in series 2.

DFT calculations were also performed for the F and BS states of the complexes in series 2, using the same functional and basis set as for series 1 (see Methods). The geometry optimization of the CuFe complex in series 2 resulted in a structure that was highly distorted

Author Manuscript Author Manuscript Author Manuscript Author Manuscript

compared to the approximately C_3 symmetric XRD structure and did not give a useful estimate for *J*. To prevent distortion, geometry optimizations were also performed for a structure of the CuFe complex with imposed C_3 symmetry, resulting in the *J* value listed in the column labeled J_{DFT} of Table 6. The latter *J* value (55 cm^{-1}) is about half the *J* value obtained by DFT for the XRD structure of the CuFe complex (125 cm^{-1}, Table 6). The disparity between the two *J* values obtained by DFT for this CuFe complex is probably related to the degeneracy of the $3d^9$ hole state of Cu and has not been further pursued. This degeneracy does not occur for the asymmetric CuFe complex of series 1. In any case, the discrepancies between J_{exp} and the two DFT values for the *J* of the CuFe complex of series 2 are small compared to the corresponding discrepancies in the case of the CuFe complex of series 1. Table 6 shows that, apart from the CuFe complex of series 2, the DFT values for *J* obtained for the XRD structures (J_{DFT}^{XRD}) are close to the DFT values for *J* obtained for the optimized geometries (J_{DFT}). The latter agreement arises when the DFT-optimized structures closely resemble those found by XRD methods.

CONCLUSION

The doubly occupied 3d-orbitals in bimetallic complexes are not “passive” but play an active role in the exchange coupling in heterometallic complexes. The *J* value of the MnFe complex in series 1 contains significant contributions from 2e-pathways involving both the t_2 and e_g orbitals of the Mn^{2+} site, while in the case of the MnFe species of series 2, the coupling is predominantly determined by the 2e-pathways emanating from one of the 3d-orbitals of metal M, viz., the e_g orbital that remains singly occupied throughout the series. This distinction implies that the increase of the total 2e-pathway contribution to *J* in the passage from the MnFe complex to the CuFe complex is compensated by 3e-pathway contributions in the case of series 1, leading to a nearly constant value for *J* throughout the series, and left virtually unchanged by 3e-pathway contributions in series 2, resulting in *J* values that increase along the series. The DFT predictions of *J* become less accurate in systems in which the 3e-pathway contributions to this parameter gain in importance because DFT underestimates the exchange energy differences between the corresponding electron-transfer excitations in the BS and F states. The *J* values obtained from both experiment and DFT suggest that the pathway parameters for the $M^{2+}Fe^{3+}$ complexes in series 1 and 2 are not strictly transferable along the two series but increase toward heavier M (Section S5). The intramolecular H-bond between the hydroxo bridge and the sulfonamide in series 1 has a significant effect on J_{DFT}, but its effect on J_{exp} is probably only minor. The mechanism by which structure causes the differences between the exchange pathways in series 1 and 2 has yet to be established.

Supplementary Material

Refer to Web version on PubMed Central for supplementary material.

ACKNOWLEDGMENTS

The work was funded by National Institutes of Health grant R01 GM077387. Funding for the EPR spectrometer was from National Science Foundation grant CHE1126268.

Author Manuscript Author Manuscript Author Manuscript Author Manuscript

REFERENCES

(1). Jiang W; Yun D; Saleh L; Barr EW; Xing G; Hoffart LM; Maslak MA; Krebs C; Bollinger JM A manganese(IV)/ iron(III) cofactor in Chlamydia trachomatis ribonucleotide reductase. Science 2007, 316, 1188–1191. [PubMed: 17525338]

(2). Fontecilla-Camps JC In Encyclopedia of Metalloproteins; Springer: New York, 2013; p 1535–1544.

(3). Schenk G; Mitic N; Gahan LR; Ollis DL; McGeary RP; Guddat LW Binuclear Metallohydrolases: Complex Mechanistic Strategies for a Simple Chemical Reaction. Acc. Chem. Res. 2012, 45, 1593–1603. [PubMed: 22698580]

(4). Diril H; Chang HR; Zhang XH; Larsen SK; Potenza JA; Pierpont CG; Schugar HJ; Isied SS; Hendrickson DN Binuclear Mixed-Valence $Mn^{II}Mn^{III}$ Complexes - Insight About the Resolution of Hyperfine-Structure in the Electron-Paramagnetic-Res Spectrum. J. Am. Chem. Soc. 1987, 109, 6207–6208.

(5). Borovik AS; Papaefthymiou V; Taylor LF; Anderson OP; Que L. Models for Iron Oxo Proteins - Structures and Properties of FeIIFeIII, ZnIIFeIII, and FeIIGaIII Complexes with (Mu-Phenoxo)Bis-(Mu-Carboxylato)Dimetal Cores. J. Am. Chem. Soc. 1989, 111, 6183–6195.

(6). Buchanan RM; Mashuta MS; Richardson JF; Oberhausen KJ; Hendrickson DN; Webb RJ; Nanny MA Synthesis, Structure, and Properties of a Novel Heterobimetallic Fe(III)Mn(II) Complex Containing a Septadentate Polyimidazole Ligand. Inorg. Chem. 1990, 29, 1299–1301.

(7). Bossek U; Hummel H; Weyhermuller T; Wieghardt K; Russell S; vanderWolf L; Kolb U. The [Mn2(IV)(mu-O)(mu-PhBO2)2]2+ unit: A new structural model for manganese-containing metalloproteins. Angew. Chem., Int. Ed. Engl. 1996, 35, 1552–1554.

(8). Ng GK; Ziller J; Borovik AS Dinuclear metal complexes with terminal hydroxo ligands as probes for the active site in the photosystem II. Abstr. Pap. Am. Chem. Soc. 2011, 241.

(9). Ng GK; Ziller JW; Borovik AS Preparation and structures of dinuclear complexes containing M^{II}-OH centers. Chem. Commun. 2012, 48, 2546–2548.

(10). Buchler S; Meyer F; Kaifer E; Pritzkow H. Tunable TACN/ pyrazolate hybrid ligands as dinucleating scaffolds for metallobiosite modeling-dinickel(II) complexes relevant to the urease active site. Inorg. Chim. Acta 2002, 337, 371–386.

(11). Isaac JA; Gennarini F; Lopez I; Thibon-Pourret A; David R; Gellon G; Gennaro B; Philouze C; Meyer F; Demeshko S; Le Mest Y; Reglier M; Jamet H; Le Poul N; Belle C. Room-Temperature Characterization of a Mixed-Valent mu-Hydroxodicopper(II,III) Complex. Inorg. Chem. 2016, 55, 8263–8266. [PubMed: 27518211]

(12). Dunn TJ; Ramogida CF; Simmonds C; Paterson A; Wong EWY; Chiang L; Shimazaki Y; Storr T. Non-Innocent Ligand Behavior of a Bimetallic Ni Schiff-Base Complex Containing a Bridging Catecholate. Inorg. Chem. 2011, 50, 6746–6755. [PubMed: 21675708]

(13). Clarke RM; Hazin K; Thompson JR; Savard D; Prosser KE; Storr T. Electronic Structure Description of a Doubly Oxidized Bimetallic Cobalt Complex with Proradical Ligands. Inorg. Chem. 2016, 55, 762–774. [PubMed: 26719989]

(14). Alliger GE; Muller P; Do LH; Cummins CC; Nocera DG Family of Cofacial Bimetallic Complexes of a Hexaanionic Carboxamide Cryptand. Inorg. Chem. 2011, 50, 4107–4115. [PubMed: 21446665]

(15). Neves A; Lanznaster M; Bortoluzzi AJ; Peralta RA; Casellato A; Castellano EE; Herrald P; Riley MJ; Schenk G. An unprecedented FeIII(mu-OH)ZnII complex that mimics the structural and functional properties of purple acid phosphatases. J. Am. Chem. Soc. 2007, 129, 7486–7487. [PubMed: 17518469]

(16). de Souza B; Kreft GL; Bortolotto T; Terenzi H; Bortoluzzi AJ; Castellano EE; Peralta RA; Domingos JB; Neves A. Second-Coordination-Sphere Effects Increase the Catalytic Efficiency of an Extended Model for $Fe^{III}M^{II}$ Purple Acid Phosphatases. Inorg. Chem. 2013, 52, 3594–3596. [PubMed: 23496379]

(17). Wong JL; Higgins RF; Bhowmick I; Cao DX; Szigethy G; Ziller JW; Shores MP; Heyduk AF Bimetallic iron-iron and iron-zinc complexes of the redox-active ONO pincer ligand. Chem. Sci. 2016, 7, 1594–1599. [PubMed: 28808535]

Author Manuscript Author Manuscript Author Manuscript Author Manuscript

(18). Rosenkoetter KE; Ziller JW; Heyduk AF A Heterobimetallic W-Ni Complex Containing a Redox-Active W-[SNS]2 Metalloligand. Inorg. Chem. 2016, 55, 6794–6798. [PubMed: 27300501]

(19). Clouston LJ; Siedschlag RB; Rudd PA; Planas N; Hu SX; Miller AD; Gagliardi L; Lu CC Systematic Variation of Metal-Metal Bond Order in Metal-Chromium Complexes. J. Am. Chem. Soc. 2013, 135, 13142–13148. [PubMed: 23901938]

(20). Eisenhart RJ; Clouston LJ; Lu CC Configuring Bonds between First-Row Transition Metals. Acc. Chem. Res. 2015, 48, 2885–2894. [PubMed: 26492331]

(21). Serrano-Plana J; Garcia-Bosch I; Company A; Costas M. Structural and Reactivity Models for Copper Oxygenases: Cooperative Effects and Novel Reactivities. Acc. Chem. Res. 2015, 48, 2397–2406. [PubMed: 26207342]

(22). Delgado M; Ziegler JM; Seda T; Zakharov LN; Gilbertson JD Pyridinediimine Iron Complexes with Pendant Redox-Inactive Metals Located in the Secondary Coordination Sphere. Inorg. Chem. 2016, 55, 555–557. [PubMed: 26692111]

(23). Barton BE; Rauchfuss TB Hydride-Containing Models for the Active Site of the Nickel-Iron Hydrogenases. J. Am. Chem. Soc. 2010, 132, 14877–14885. [PubMed: 20925337]

(24). Greenwood BP; Forman SI; Rowe GT; Chen CH; Foxman BM; Thomas CM Multielectron Redox Activity Facilitated by Metal-Metal Interactions in Early/Late Heterobimetallics: Co/Zr Complexes Supported by Phosphinoamide Ligands. Inorg. Chem. 2009, 48, 6251–6260. [PubMed: 19499941]

(25). Krogman JP; Thomas CM Metal-metal multiple bonding in C3-symmetric bimetallic complexes of the first row transition metals. Chem. Commun. 2014, 50, 5115–5127.

(26). Wu B; Wilding MJT; Kuppuswamy S; Bezpalko MW; Foxman BM; Thomas CM Exploring Trends in Metal-Metal Bonding, Spectroscopic Properties, and Conformational Flexibility in a Series of Heterobimetallic Ti/M and V/M Complexes (M = Fe, Co, Ni, and Cu). Inorg. Chem. 2016, 55, 12137–12148. [PubMed: 27571456]

(27). Sano Y; Lau N; Weitz AC; Ziller JW; Hendrich MP; Borovik AS Models for Unsymmetrical Active Sites in Metal-loproteins: Structural, Redox, and Magnetic Properties of Bimetallic Complexes with MII(mu-OH)FeIII Cores. Inorg. Chem. 2017, 56, 14118–14128. [PubMed: 29112385]

(28). Dawson JW; Wang RH; Schredder JM; Rossman GR; Gray HB; Hoenig HE Magnetic Susceptibility Study of Hemerythrin Using an Ultrasensitive Magnetometer. Biochemistry 1972, 11, 461–465. [PubMed: 5059123]

(29). Weitz AC; Giri N; Caranto JD; Kurtz DM; Bominaar EL; Hendrich MP Spectroscopy and DFT Calculations of a Flavodiiron Enzyme 1mplicate New Diiron Site Structures. J. Am. Chem. Soc. 2017, 139, 12009–12019. [PubMed: 28756660]

(30). Biswas B; Salunke-Gawali S; Weyhermuller T; Bachler V; Bill E; Chaudhuri P. Metal-Complexes As Ligands to Generate Asymmetric Homo- and Heterodinuclear MAIIIMBII Species: a Magneto-Structural and Spectroscopic Comparison of 1midazole-N versus Pyridine-N. Inorg. Chem. 2010, 49, 626–641. [PubMed: 20000374]

(31). Eremin MV; Kalinenkov VN; Rakitin YV 2-Center Exchange 1nteractions between Orbitally Degenerate 1ons. 1. One 1on in Orbitally Degenerate State. Phys. Status Solidi B 1978, 89, 503–512.

(32). Eremin MV; Kalinenkov VN; Rakitin YV 2-Center Exchange Interactions between Orbitally Degenerate 1ons. 2. 1ons in Orbitally Degenerate States. Phys. Status Solidi B 1978, 90, 123–134.

(33). Eremin MV; Kalinenkov VN; Rakitin YV Exchange 1nteraction of Cu^{2+} and Mn^{2+} 1ons in KZnF3. Fiz. Tverd. Tela. 1978, 20, 2832–2834.

(34). Eremin MV; Rakitin YV Channel Model in Isotropic Exchange Theory. Phys. Status Solidi B 1977, 80, 579–587.

(35). Eremin MV; Rakitin YV Channel Model in 1sotropic Exchange Theory 2. Phys. Status Solidi B 1977, 82, 221–228.

(36). Eremin MV; Rakitin YV Channel Model in Isotropic Exchange Theory 3. Phys. Status Solidi B 1978, 85, 783–788.

Author Manuscript Author Manuscript Author Manuscript Author Manuscript

(37). Rakitin IV; Eremin MV; Kalinnikov VT Model of Channels in Theory of Exchange. Dokl. Akad. Nauk SSSR 1977, 233, 327–329.

(38). Rakitin IV; Kalinnikov VT; Eremin MV Cleavage in Zero-Field and Exchange Interaction in Dimeric Copper Carboxilates. Dokl. Akad. Nauk SSSR 1978, 241, 877–879.

(39). Rakitin YV; Kalinnikov VT; Eremin MV Mechanisms of Exchange Interactions in Some Transition-Metal Carboxylates, Sulfates, and Chlorides. Theor. Chim. Acta 1977, 45, 167–176.

(40). De Jongh LJ; Block R Exchange 1nteractions in Some 3 d-Metal 1onic Compounds. 1. 180 Degrees Superexchange in 3d-Metal Fluorides XMF3 and X2MF4 (X = K,Rb,Tl-M = Mn,Co,Ni). Physica B & C 1975, 79, 568–593.

(41). Noodleman L; Case DA Density-Functional Theory of Spin Polarization and Spin Coupling in Iron-Sulfur Clusters. Adv. inorg. Chem. 1992, 38, 423–458.

(42). Goodenough JB Theory of the Role of Covalence in the Perovskite-Type Manganites [La,M(II)]MnO3. Phys. Rev. 1955, 100, 564–573.

(43). Goodenough JB An 1nterpretation of the Magnetic Properties of the Perovskite-Type Mixed Crystals La1–xSrxCoO$_{3-\lambda}$. J. Phys. Chem. Solids 1958, 6, 287–297.

(44). Goodenough JB Magnetism and the Chemical Bond; Wiley: New York, 1963.

(45). Anderson PW New Approach to the Theory of Super-exchange 1nteractions. Phys. Rev. 1959, 115, 2–13.

(46). Anderson PW In Magnetism; Rado GT, Suhl H, Eds.; Academic: New York, 1963; Vol. I, p 25.

(47). Anderson PW In Solid State Physics; Seitz F, Turnbull D, Eds.; Academic: New York, 1963; Vol. 14, p 99.

(48). Kanamori J. Superexchange 1nteraction and Symmetry Properties of Electron Orbitals. J. Phys. Chem. Solids 1959, 10, 87–98.

(49). Bominaar EL; Block R. Numerical Comparison between the Channel Model and the Effective-Electron Model Descriptions of Linear Superexchange 1nteractions in Ionic Solids. Phys. Rev. B: Condens. Matter Mater. Phys. 1986, 33, 3672–3677.

(50). Bominaar EL; Block R. Channel Decomposition of Superexchange 1nteractions in the Valence-Bond Method. Phys. Rev. B: Condens. Matter Mater. Phys. 1986, 34, 515–520.

(51). Anderson PW; Hasegawa H. Considerations on Double Exchange. Phys. Rev. 1955, 100, 675–681.

(52). Zener C. 1nteraction between the D-Shells in the Transition Metals. Phys. Rev. 1951, 81, 440–444.

(53). Borshch SA; Bominaar EL; Blondin G; Girerd JJ Double Exchange and Vibronic Coupling in Mixed-Valence Systems - Origin of the Broken-Symmetry Ground-State of $[Fe_3S_4]^0$ Cores in Proteins and Models. J. Am. Chem. Soc. 1993, 115, 5155–5168.

(54). Bominaar EL; Borshch SA; Girerd JJ Double-Exchange and Vibronic Coupling in Mixed-Valence Systems - Electronic-Structure of $[Fe_4S_4]^{3+}$ Clusters in High-Potential 1ron Protein and Related Models. J. Am. Chem. Soc. 1994, 116, 5362–5372.

(55). Malrieu JP; Caballol R; Calzado CJ; de Graaf C; Guihery N. Magnetic 1nteractions in Molecules and Highly Correlated Materials: Physical Content, Analytical Derivation, and Rigorous Extraction of Magnetic Hamiltonians. Chem. Rev. 2014, 114, 429–492. [PubMed: 24102410]

(56). Frisch MJ; Trucks GW; Schlegel HB; Scuseria GE; Robb MA; Cheeseman JR; Scalmani G; Barone V; Petersson GA; Nakatsuji H; Li X; Caricato M; Marenich A; Bloino J; Janesko BG; Gomperts R; Mennucci B; Hratchian HP; Ortiz JV; Izmaylov AF; Sonnenberg JL; Williams-Young D; Ding F; Lipparini F; Egidi F; Goings J; Peng B; Petrone A; Henderson T; Ranasinghe D; Zakrzewski VG; Gao J; Rega N; Zheng G; Liang W; Hada M; Ehara M; Toyota K; Fukuda R; Hasegawa J; Ishida M; Nakajima T; Honda Y; Kitao O; Nakai H; Vreven T; Throssell K; Montgomery JA Jr.; Peralta JE; Ogliaro F; Bearpark M; Heyd JJ; Brothers E; Kudin KN; Staroverov VN; Keith T; Kobayashi R; Normand J; Raghavachari K; Rendell A; Burant JC; Iyengar SS; Tomasi J; Cossi M; Millam JM; Klene M; Adamo C; Cammi R; Ochterski JW; Martin RL; Morokuma K; Farkas O; Foresman JB; Fox DJ Gaussian 09; Gaussian, Inc.: Wallingford, CT, 2016.

(57). Becke AD A New Mixing of Hartree-Fock and Local Density-Functional Theories. J. Chem. Phys. 1993, 98, 1372–1377.

Author Manuscript Author Manuscript Author Manuscript Author Manuscript

(58). Lee CT; Yang WT; Parr RG Development of the Colle-Salvetti Correlation-Energy Formula into a Functional of the Electron-Density. Phys. Rev. B: Condens. Matter Mater. Phys. 1988, 37, 785–789.

(59). Comba P; Hausberg S; Martin B. Calculation of Exchange Coupling Constants of Transition Metal Complexes with DFT. J. Phys. Chem. A 2009, 113, 6751–6755. [PubMed: 19469514]

(60). Mclean AD; Chandler GS Contracted Gaussian-Basis Sets for Molecular Calculations. 1. 2nd Row Atoms, Z = 11–18. J. Chem. Phys. 1980, 72, 5639–5648.

(61). Krishnan R; Binkley JS; Seeger R; Pople JA Self-Consistent Molecular-Orbital Methods. 20. Basis Set for Correlated Wave-Functions. J. Chem. Phys. 1980, 72, 650–654.

(62). Schaefer A; Horn H; Ahlrichs R. Fully Optimized Contracted Gaussian-Basis Sets for Atoms Li to Kr. J. Chem. Phys. 1992, 97, 2571–2577.

(63). Schaefer A; Huber C; Ahlrichs R. Fully Optimized Contracted Gaussian-Basis Sets of Triple Zeta Valence Quality for Atoms Li to Kr. J. Chem. Phys. 1994, 100, 5829–5835.

(64). Weigend F; Ahlrichs R. Balanced basis sets of split valence, triple zeta valence and quadruple zeta valence quality for H to Rn: Design and assessment of accuracy. Phys. Chem. Chem. Phys. 2005, 7, 3297–3305. [PubMed: 16240044]

(65). Fuentealba P. On the Reliability of Semi-Empirical Pseudopotentials - Dipole Polarizability of the Alkali Atoms. J. Phys. B: At. Mol. Phys. 1982, 15, L555–L558.

(66). Fuentealba P; Preuss H; Stoll H; Vonszentpaly L. A Proper Account of Core-Polarization with Pseudopotentials - Single Valence-Electron Alkali Compounds. Chem. Phys. Lett. 1982, 89, 418–422.

(67). Fuentealba P; Stoll H; Von Szentpaly L; Schwerdtfeger P; Preuss H. On the Reliability of Semi-Empirical Pseudopotentials - Simulation of Hartree-Fock and Dirac-Fock Results. J. Phys. B-At. Mol. Opt. 1983, 16, L323–L328.

(68). Fuentealba P; Von Szentpaly L; Stoll H; Fraschio FX; Preuss H. Pseudopotential Calculations Including Core-Valence Correlation - Alkali Compounds. J. Mol. Struc.-Theochem. 1983, 93, 213–219.

(69). Dolg M; Stoll H; Preuss H. Energy-Adjusted Abinitio Pseudopotentials for the Rare-Earth Elements. J. Chem. Phys. 1989, 90, 1730–1734.

(70). Dolg M; Wedig U; Stoll H; Preuss H. Abinitio Pseudopotential Study of the 1st Row Transition-Metal Monoxides and Iron Monohydride. J. Chem. Phys. 1987, 86, 2123–2131.

(71). Dolg M; Wedig U; Stoll H; Preuss H. Energy-Adjusted Abinitio Pseudopotentials for the 1st-Row Transition-Elements. J. Chem. Phys. 1987, 86, 866–872.

(72). Jullien J; Juhasz G; Mialane P; Dumas E; Mayer CR; Marrot J; Riviere E; Bominaar EL; Munck E; Secheresse F. Structure and magnetic properties of a non-heme diiron complex singly bridged by a hydroxo group. Inorg. Chem. 2006, 45, 6922–6927. [PubMed: 16903750]

(73). Gerloch M; Mabbs FE Crystal and Molecular Structure of Chloro-(NN'-Bis-Salicylidene-Ethylenediamine) Iron(3) as a Hexaco-Ordinate Dimer. J. Chem. Soc. A 1967, 1900–1908.

(74). Menage S; Que L. A Bis(Mu-Alkoxo)Diiron Complex with Novel Terminally Ligated Carboxylates. Inorg. Chem. 1990, 29, 4293–4297.

(75). Chiari B; Piovesana O; Tarantelli T; Zanazzi PF Exchange Interaction in Multinuclear Transition-Metal Complexes. 6. Nature of Metal Metal Coupling in Dinuclear Iron(III) Systems Containing Fe-O-Fe-O Bridging Units. Inorg. Chem. 1984, 23, 3398–3404.

(76). Murch BP; Bradley FC; Boyle PD; Papaefthymiou V; Que L. Iron-Oxo Aggregates - Crystal-Structures and Solution Characterization of 2-Hydroxy-1,3-Xylylenediaminetetraacetic Acid Complexes. J. Am. Chem. Soc. 1987, 109, 7993–8003.

(77). Borer L; Thalken L; Ceccarelli C; Glick M; Zhang JH; Reiff WM Synthesis and Characterization of a Hydroxyl-Bridged Iron(lIl) Dimer of N,N'-Ethylenebis(Salicylamine). Inorg. Chem. 1983, 22, 1719–1725.

(78). Armstrong WH; Lippard SJ Reversible Protonation of the Oxo Bridge in a Hemerythrin Model-Compound - Synthesis, Structure, and Properties of (Mu-Hydroxo)Bis(Mu-Acetato)Bis-[Hydrotris(1-Pyrazolyl) Borato]Diiron(III), [(Hb(Pz)3) Fe(OH)-(O2CCH3)2Fe(Hb(Pz)3)]+. J.Am. Chem. Soc. 1984, 106,4632–4633.

Author Manuscript Author Manuscript Author Manuscript Author Manuscript

(79). Wieghardt K; Bossek U; Nuber B; Weiss J; Bonvoisin J; Corbella M; Vitols SE; Girerd JJ Synthesis, Crystal-Structures, Reactivity, and Magnetochemistry of a Series of Binuclear Complexes of Manganese(II), Manganese(III), and Manganese(IV) of Biological Relevance - the Crystal-Structure of [L'MnIV(Mu-O)3MnIVL';]-(PF6)2.H2O Containing an Unprecedented Short Mn···Mn Distance of 2.296 Å. J. Am. Chem. Soc. 1988, 110, 7398–7411.

(80). Holman TR; Wang ZG; Hendrich MP; Que L. Structural and Spectroscopic Properties of Antiferromagnetically Coupled Fe(III)Mn(II) and Fe(II)Mn(II) Complexes. Inorg. Chem. 1995, 34, 134–139.

(81). Holman TR; Juarez-Garcia C; Hendrich MP; Que L; Munck E. Models for Iron Oxo Proteins - Mossbauer and Epr Study of an Antiferromagnetically Coupled $Fe^{III}Ni^{II}$ Complex. J. Am. Chem. Soc. 1990, 112, 7611–7618.

(82). Holman TR; Andersen KA; Anderson OP; Hendrich MP; Juarezgarcia C; Munck E; Que L. Correlations between Magnetism and Structure in Dinuclear $Cu^{II}Fe^{III}$ Complexes with Integer Spin EPR Signals. Angew. Chem., Int. Ed. Engl. 1990, 29, 921–923.

(83). Journaux Y; Kahn O; Zarembowitch J; Galy J; Jaud J. Symmetry of the Magnetic Orbitals and Exchange Interaction in $Cu^{II}Fe^{III}$ and $Cu^{II}Cr^{III}$ Heterobinuclear Complexes - Crystal-Structure of CuFe[(FSA)2En]Cl(H2O)(Ch3OH).CH3OH. J. Am. Chem. Soc. 1983, 105, 7585–7591.

(84). Oberhausen KJ; Richardson JF; O'Brien RJ; Buchanan RM; McCusker JK; Webb RJ; Hendrickson DN Attenuation of Antiferromagnetic Exchange Interactions Via H_2O Hydrogen-Bonding to Oxo-Bridged Diiron(III) Complexes. Inorg. Chem. 1992, 31, 1123–1125.

(85). Bruijnincx PCA; Buurmans ILC; Huang YX; Juhasz G; Viciano-Chumillas M; Quesada M; Reedijk J; Lutz M; Spek AL; Munck E; Bominaar EL; Klein Gebbink RJM Mono- and Dinuclear Iron Complexes of Bis(1-methylimidazol-2-yl)ketone (bik): Structure, Magnetic Properties, and Catalytic Oxidation Studies. Inorg. Chem. 2011, 50, 9243–9255. [PubMed: 21902227]

(86). Hujo W; Grimme S. Comparison of the performance of dispersion-corrected density functional theory for weak hydrogen bonds. Phys. Chem. Chem. Phys. 2011, 13, 13942–13950. [PubMed: 21594296]

(87). Boys SF; Bernardi F. Calculation of Small Molecular Interactions by Differences of Separate Total Energies - Some Procedures with Reduced Errors. Mol. Phys. 1970, 19, 553–566.

(88). Simon S; Duran M; Dannenberg JJ How does basis set superposition error change the potential surfaces for hydrogen bonded dimers? J. Chem. Phys. 1996, 105, 11024–11031.

(89). Yamashita J; Kondo J. Superexchange Interaction. Phys. Rev. 1958, 109, 730–741.

(90). Brink DN; Satchler G. R Angular Momentum, 3rd ed.; Clarendon Press: Oxford, UK, 1994.

Author Manuscript Author Manuscript Author Manuscript Author Manuscript

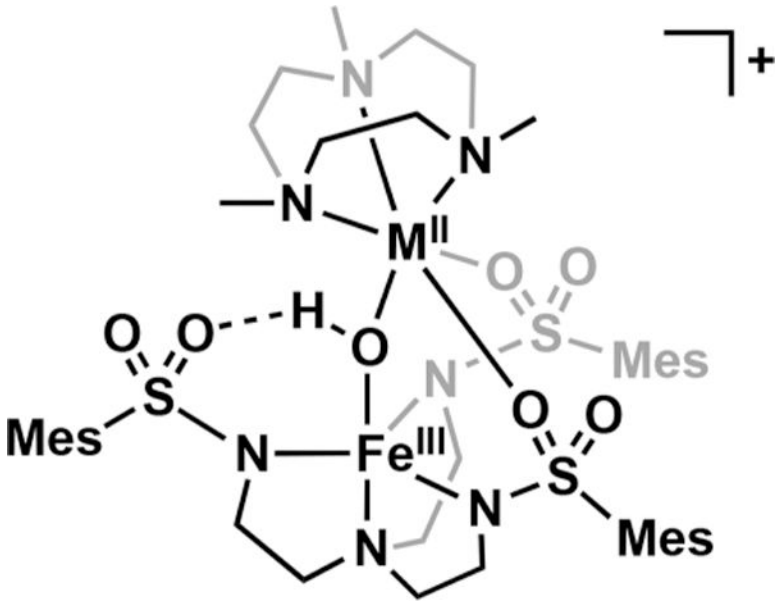

Figure 1.

Structure of the $[M^{2+}Fe^{3+}]^{+}$ complexes, M = Mn, Fe, Ni, and Cu, of series 1. Mes is for mesityl.

Author Manuscript Author Manuscript Author Manuscript Author Manuscript

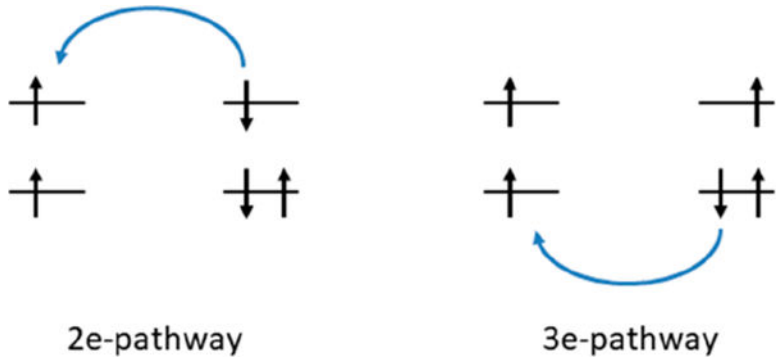

Figure 2.

Intermetal electron-transfer pathways: 2e-pathway (left) and 3e-pathway (right). The 2e- and 3e-pathways involve the transfer of an unpaired electron and paired electron and favor antiparallel and parallel spin alignment, respectively.

Author Manuscript Author Manuscript Author Manuscript Author Manuscript

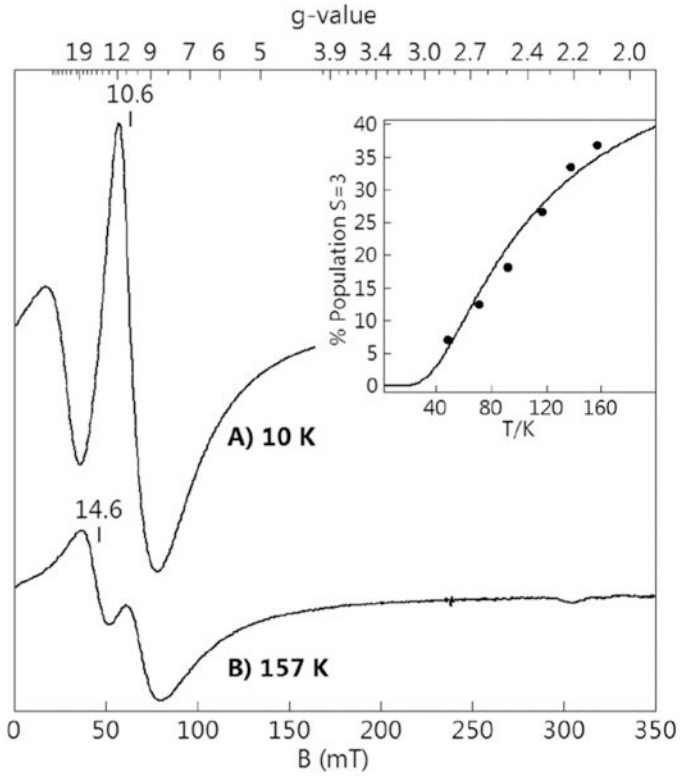

Figure 3.

Parallel-mode EPR spectra (9.405 GHz, 0.2 mW) of the CuFe complex of series 1 in powder at temperatures of (A) 10 K and (B) 157 K. The inset shows a plot of the product of the signal times temperature versus temperature of the g = 14.6 signal (●) and a fit to the population of the excited $S = 3$ multiplet for $J = 35(5)$ cm^{-1}.

Author Manuscript Author Manuscript Author Manuscript Author Manuscript

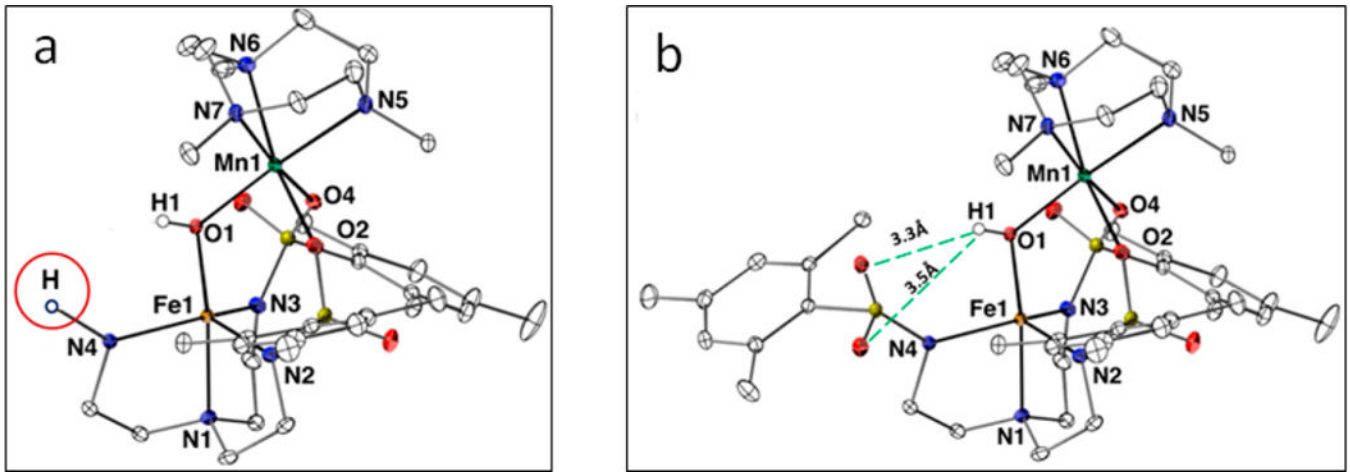

Figure 4.

Modified structures of the MnFe complex of series 1 in which the H-bond was removed by (a) cleavage of the N4–S bond and replacement of the sulfonamido group by a hydrogen atom (encircled in red) and (b) rotation over dihedral angle Fe–N4–S–O6.

Author Manuscript Author Manuscript Author Manuscript Author Manuscript

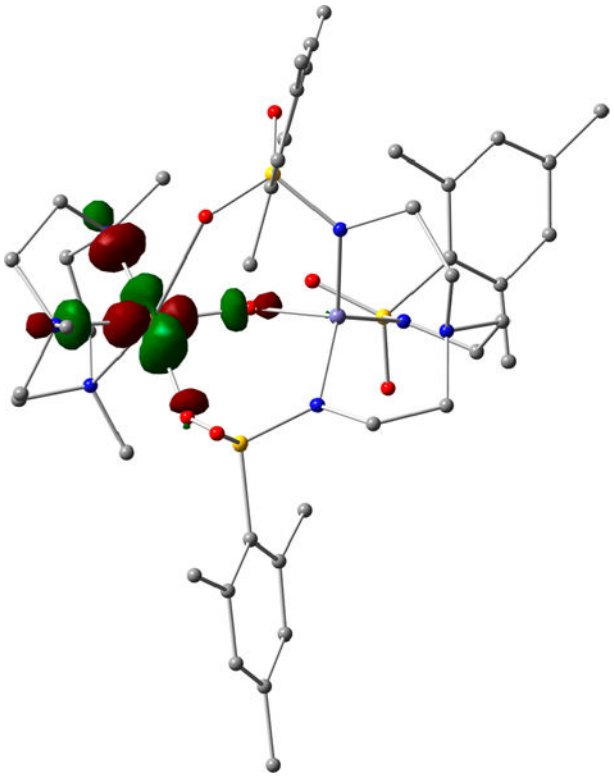

Figure 5.

Contour plot of the α-LUMO in the BS state, orbital 256α, containing the hole in the $3d^9$ configuration $(xy)^2\ (xz)^2\ (yz)^2\ (z^2)^2\ (x^2 - y^2)^\beta$ of Cu^{2+} in the CuFe complex of series 1.

Author Manuscript Author Manuscript Author Manuscript Author Manuscript

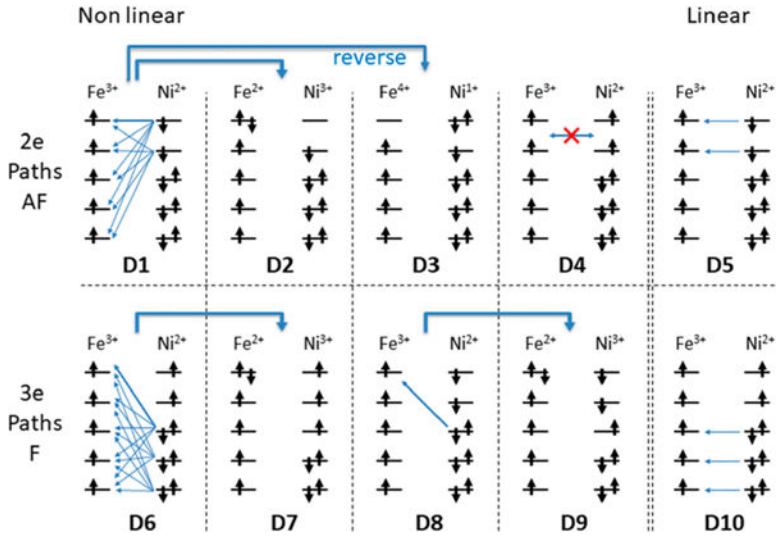

Figure 6.

Interactions of the ground configuration with electron-transfer configurations in the $Fe^{3+}Ni^{2+}$ complex that give ferro- and antiferromagnetic contributions to J in low and high symmetry (D5, D10) systems.

Author Manuscript

Author Manuscript

Author Manuscript

Author Manuscript

Table 1.

Basis Sets Used for Calculating J in the MnFe Complex of Series 1

	atomic basis sets				
basis set	**H, C, N**	**O, S, H_{bridge}**	**Fe^{III}, Mn^{II}**	**dielectric constant, ε**	**J, cm^{-1}**
1	6-311G	6-311G	6-311G	1	63
2	TZVP	TZVP	TZVP	1	52
3	6-311G	TZVP	TZVP	1	52
	6-311G	TZVP	TZVP	8.93[a]	48
4	6-311G	TZVP	SDD	1	46
	6-311G	TZVP	SDD	8.93[a]	42
		from EPR in DCM/THF			33(3)

[a]The ε value for DCM, which is only slightly larger than the ε of 7.58 for THF, was used for describing the solvent mixture.

Author Manuscript

Author Manuscript

Author Manuscript

Author Manuscript

Table 2.

Comparison of J_{exp} with J_{DFT} (Basis Set 4, $\varepsilon = 8.93$) Obtained with and without Hydrogen Bonding (HB)

		J_{DFT} cm^{-1}		
complex of series 1	**J_{exp}, cm^{-1}**	**complete structure with HB[a]**	**structure Figure 4a: no HB[b]**	**structure Figure 4b: no HB[c]**
$Mn^{2+}Fe^{3+}$	33(3)	42	34	39
$Fe^{2+}Fe^{3+}$	26(4)	47	23	37
$Ni^{2+}Fe^{3+}$	35(5)	53	39	50
$Cu^{2+}Fe^{3+}$	33(5)	141	126	123

[a] E_{BS} and E_F from unconstrained optimizations of the complete structure.

[b] E_{BS} and E_F from single point calculations of the truncated structure in Figure 4a.

[c] E_{BS} and E_F from dihedral-angle-constrained optimizations of the complete structure.

Author Manuscript Author Manuscript Author Manuscript Author Manuscript

Table 3.

Selected XRD vs DFT Bond Distances (Å) and Angles (degrees) for $[M^{II}\text{-}(\mu\text{-OH})\text{-}Fe^{III}]^{+}$ Complexes of Series 1

	Mn^{II}		Fe^{II}		Ni^{II}		Cu^{II}	
parameters	**XRD**	**DFT**	**XRD**	**DFT**	**XRD**	**DFT**	**XRD**	**DFT**
Fel–Ol	1.888(1)	1.914	1.899(2)	1.930	1.884(2)	1.911	1.892(5)	1.929
O1···O6	2.646(2)	2.668	2.649(2)	2.655	2.644(3)	2.662	2.622(7)	2.665
Ml–Ol	2.048(1)	2.065	1.986(2)	1.988	1.970(2)	1.990	1.905(5)	1.926
Fel···Ml	3.447(1)	3.551	3.425(1)	3.524	3.416(1)	3.511	3.422(1)	3.524
Fel–Ol–Ml	122.2(7)	126.3	124.3(9)	128.1	124.8(1)	127.6	128.1(3)	132.1

Inorg Chem. Author manuscript; available in PMC 2019 October 12.

Author Manuscript Author Manuscript Author Manuscript Author Manuscript

Table 4.

Decomposition of J in Series 1 in Antiferromagnetic (2e-Pathway) and Ferromagnetic (3e-Pathway) Contributions in the Case of Non-Hund's Rule States with Infinite Energy[a]

dimer	J_{exp}	$N_A N_B J_{exp}$	$N_A N_B j_{av}^{AF}$	$25 - N_A N_B J_{av}^{F}$	Δ_M	j_{av}^{AF} **b**	j_{av}^{F} **b**
$Fe^{3+}Mn^{2+}$	33	825	825	0	0	33	0
$Fe^{3+}Fe^{2+}$	30[c]	600	$825 - \Delta_{Fe}$	$-(8/5)\Delta_{Fe}$	87	37	–28
$Fe^{3+}Ni^{2+}$	35	350	$825 - 3\Delta_{Ni}$	$-4\Delta_{Ni}$	68	62	–18
$Fe^{3+}Cu^{2+}$	33	165	$825 - 4\Delta_{Cu}$	$-4\Delta_{Cu}$	83	99	–17

[a] All energies in cm^{-1}.

[b] For example, J for M = Ni^{2+} is obtained from j_{av}^{AF} and j_{av}^{F} as $J_{exp} = \left(10 j_{av}^{AF} + 15 j_{av}^{F}\right)/10$.

[c] Upper bound of experiment.

Author Manuscript

Author Manuscript

Author Manuscript

Author Manuscript

Table 5.

Number of Ferromagnetic Contributions from 3e-Pathways (F) and Potential Exchange (F_{pe}[a]) and Antiferromagnetic (AF) 2e-Pathway Contributions to J in Linear Bridged Hetero- and Homometal Complexes[a]

hetero	AF	F_{pe}	F	homo	AF	F_{pe}	F
$Fe^{3+}Mn^{2+}$	5	25	0	$Mn^{2+}Mn^{2+}$	5	25	0
$Fe^{3+}Fe^{2+}$	4	20	1	$Fe^{2+}Fe^{2+}$	4	16	0
$Fe^{3+}Ni^{2+}$	2	10	3	$Ni^{2+}Ni^{2+}$	2	4	0
$Fe^{3+}Cu^{2+}$	1	5	4	$Cu^{2+}Cu^{2+}$	1	1	0

[a]Ferromagnetic exchange, referred to as “potential exchange” (PE) by Anderson.[46] As PE terms are also present for pathways with $b_{ik} \neq 0$, they have been included in the count as well although they are weaker than the antiferromagnetic contribution to the same pathway.

Author Manuscript

Author Manuscript

Author Manuscript

Author Manuscript

Table 6.

Comparison of J Values (cm^{-1}) from Experiment and DFT for Mixed-Metal Complexes

	series 1			series 2		
M	J_{exp} [a]	J_{DFT} [b]	J_{DFT} XRD [c]	J_{exp} [d]	J_{DFT}	J_{DFT} XRD [c]
Mn	33	42	52	15	19	20
Ni	35	53	51	57	70	70
Cu	33	141	138	76	55 [e]	125

[a] Obtained from EPR in ref 27 and this work.

[b] This work, using energies for optimized structures for the F and BS states before correcting for the overestimated effect of H-bonding on *J*.

[c] Using X-ray diffraction structures.

[d] Obtained from magnetic susceptibility, ref 30.

[e] Using optimized structures for F and BS states with imposed C_3 symmetry.